Icarus 227 (2014) 8–20

Contents lists available at ScienceDirect

Icarus

journal homepage: www.elsevier.com/locate/icarus

The horizontal motion of dust devils on Mars derived from CRISM and CTX/HiRISE observations

D. Reiss [a,*], A. Spiga [b], G. Erkeling [a]

[a] Institut für Planetologie, Westfälische Wilhelms-Universität, Wilhelm-Klemm-Str. 10, 48149 Münster, Germany
[b] Laboratoire de Météorologie Dynamique, Université Pierre et Marie Curie, Paris, France

ARTICLE INFO

Article history:
Received 11 February 2013
Revised 29 August 2013
Accepted 31 August 2013
Available online 10 September 2013

Keywords:
Mars, atmosphere
Mars, climate
Mars, surface
Terrestrial planets
Atmospheres, dynamics

ABSTRACT

We derived the horizontal motion (speed and direction) of dust devils from time-delayed Mars Reconnaissance Orbiter (MRO) coordinated image data sets of the Compact Reconnaissance Imaging Spectrometer for Mars (CRISM) to the Context Camera (CTX) and/or the High Resolution Imaging Science Experiment (HiRISE) acquired between 2008 and 2011. In total, 47 dust devils were observed in 15 regions with diameters ranging from 15 to 280 m with an average diameter of 100 m and heights from 40 to 4400 m. Horizontal speeds of 44 dust devils range from 4 to 25 ms^{-1} with average speeds of 12 ms^{-1}. The majority of dust devils were observed in the northern hemisphere (79%), mainly in Amazonis Planitia (67.5% from the northern hemisphere dust devils). Seasonal occurrence of dust devils in the northern hemisphere is predominant in early and mid spring (76%). We compared our measured dust devil horizontal speeds and directions of motion to the monthly climatologies (wind speed and direction) released in the Mars Climate Database (MCD) derived from General Circulation Model (GCM) predictions. There is a broad agreement between dust devil horizontal speeds and MCD wind speed predictions within the Planetary Boundary Layer (PBL) as well as dust devil directions of motion and MCD predicted wind directions occurring within the PBL. Comparisons between dust devil horizontal speeds and MCD near-surface wind speed predictions at 10 m height above the surface do not correlate well: dust devils move about a factor of 2 faster than MCD near-surface wind predictions. The largest offsets between dust devil motion and MCD predictions were related to three dust devils occurring near the Phoenix landing site when the lander was still active. The offsets could be explained by a regional weather front passing over the Phoenix landing site. In general, the good agreement between dust devil horizontal speeds and directions of motion, and ambient wind speeds and directions predicted within the PBL through GCM, show that dust devils on Mars move with ambient winds in the PBL, hence faster than near surface winds.

1. Introduction

Dust-laden vortices known as dust devils are common in semi-arid and arid regions on Earth (e.g., Balme and Greeley, 2006). On Mars, active dust devils were first observed in satellite imagery by Thomas and Gierasch (1985) and in lander images by Metzger et al. (1999). Recent satellite and lander missions confirmed that dust devils occur frequently on Mars (e.g., Cantor et al., 2006; Stanzel et al., 2008; Greeley et al., 2010; Choi and Dundas, 2011). They play a potentially key role in maintaining and replenishing the background dust opacity in the martian atmosphere (e.g., Newman et al., 2002; Whelley and Greeley, 2008). Dust devils cause erosion of thin dust layers on the surface which lead to lower albedo tracks compared to the unaltered background (e.g., Greeley et al., 2005; Reiss et al., 2010), although some dust devil tracks on Mars show a higher albedo (bright tracks) compared to its surroundings (e.g., Malin and Edgett, 2001; Cantor et al., 2006; Reiss et al., 2011a). Better knowledge of dust devils' physical parameters is necessary to understand their influence on the martian atmosphere, climate and surface changes.

We define the speed and direction of dust devils moving horizontally across the martian surface to the term 'horizontal motion', and using 'horizontal speed' and 'direction of motion' to refer to magnitude and direction of the horizontal motion, respectively. We use this terminology to avoid confusion with wind vectors (e.g., horizontal, vertical, radial, and tangential velocities) within dust devils. The used 'horizontal speed' in this paper is equivalent to the terms 'horizontal speed' in Greeley et al. (2006, 2010), 'traverse velocity' and 'traverse speed' in Stanzel et al. (2008) and Reiss et al. (2011b), and 'ground speed' in Balme et al. (2012).

Horizontal motion (speed and direction) of martian dust devils were derived thus far from lander and rover observations (Metzger et al., 1999; Greeley et al., 2006, 2010) and High Resolution Stereo

* Corresponding author.
E-mail address: dennis.reiss@uni-muenster.de (D. Reiss).

0019-1035/$ - see front matter © 2013 Elsevier Inc. All rights reserved.
http://dx.doi.org/10.1016/j.icarus.2013.08.028

Camera (HRSC) satellite imagery (Stanzel et al., 2006, 2008; Reiss et al., 2011b). Cantor et al. (2006) also retrieved the horizontal motion and tangential speed of one dust devil using Viking Orbiter image frames. Recently, tangential speeds (vortex winds) and estimates of horizontal motion of dust devils were also retrieved from HiRISE images by Choi and Dundas (2011).

Early field observations on Earth suggested that dust devils move across the surface with horizontal speeds which, to first order, correspond to ambient wind fields (e.g., Wegener, 1914; Flower, 1936; Crozier, 1970). The more recent and detailed terrestrial field measurements of Balme et al. (2012) showed that dust devil horizontal speed is in agreement with wind speeds a few tens of meters above the surface, and that their horizontal direction closely matches ambient wind directions. However, the study also showed that dust devils move about 10–20% faster than ambient wind speeds measured at 10 m height above the surface (Balme et al., 2012). These results suggest that the horizontal motion of terrestrial dust devils can be used as a proxy for PBL wind speeds and directions (Balme et al., 2012). As pointed out by those authors, there should be no physical reason why this relationship would differ on Mars. Preliminary tests using a few measurements indicated indeed a broad agreement between dust devil horizontal speeds (Stanzel et al., 2006) and directions (Stanzel et al., 2008) with ambient wind speeds and directions through Global Climate Models (GCMs).

Here we introduce a new technique to derive horizontal motions for martian dust devils using image data from the Compact Reconnaissance Imaging Spectrometer for Mars (CRISM) (Murchie et al., 2007) together with time delayed image observations by the Context Camera (CTX) (Malin et al., 2007) and/or High Resolution Imaging Science Experiment (HiRISE) (McEwen et al., 2007). This is the first time this combination of instruments on board Mars Reconnaissance Orbiter (MRO) is used to retrieve the characteristics of dust devils. We then compare the obtained dust devil horizontal speeds and directions of motion to the monthly climatologies released in the Mars Climate Database (Lewis et al., 1999; Millour et al., 2008) and derived from GCM predictions to ascertain whether dust devils on Mars behave like their terrestrial counterparts.

2. Data and methods

While the CTX and HiRISE (red channel) instrument image the same spot on the martian surface at nearly identical times, CRISM uses a specific imaging technique which results in larger time offsets to the other imaging instruments onboard MRO. The CRISM instrument uses an active pointing device, a gimbaled sensor system enabling that a target can be tracked with long exposure time. During an observation the center of a surface target is imaged in forward looking, nadir, and backward looking angles in flight direction commanded by the Gimbal Motor Electronics (GME) unit (for further details see Murchie et al. (2007)). This imaging technique results in positive and negative time offsets (±1 min) from the center of the surface target to the simultaneously in flight direction scanning HiRISE and CTX instruments (Fig. 1). We calculated the exact acquisition time of the center of dust devils in CRISM raw images using the start and stop time of the image acquisition in combination with the image line position of the dust devil center. For each CRISM image line the exact spacecraft clock time is recorded in tabular files, hence the time elapsed after the image start time can be calculated. Imaging times of equivalent dust devils in CTX or HiRISE images were read out in the ISIS (Torson and Becker, 1997) image viewer QView after ISIS3 processing.

For our analysis we used image data from CRISM, CTX and HiRISE, all mounted on a platform onboard Mars Reconnaissance Orbiter (MRO). CRISM acquires targeted hyperspectral images at full spatial resolution with 18 m/pxl (FRT), and half resolution short (HRS) as well as half resolution long (HRL) images with spatial resolutions of 36 m/pxl (Murchie et al., 2007). We did a systematic dust devil survey based on all available CRISM center targeted (FRT, HRS, and HRL) VNIR false color RGB browse images available at PDS Geoscience Node (Washington University in St. Louis; http://ode.rsl.wustl.edu/mars/datafiles/mro-m-crism-3-rdr-targeted-v1/browse/) released until 01 October 2012. After finding dust devils in browse images, we processed the raw images containing dust devils with the Environment for the Visualization of Images (ENVI) (Exelis Visual Information Solutions, 2013). Images were pre-processed with the CRISM Analysis Tool (CAT) (Seelos and the CRISM Team, 2009) and were corrected for instrumental, atmospheric and photometric effects. The map projected CRISM images were then exported from ENVI for measurements in ArcGIS 9.3. It is noteworthy that there is no significant visual difference between the ENVI processed raw CRISM images and the false color RGB browse images which were used for our systematic dust devil search. In addition to dust devils found in the released CRISM browse products, we processed CRISM raw images when no browse images were available based on known active dust devils imaged by HiRISE.

The optical properties of all three instruments differ, which might affect our dust devil identification and measurements. CRISM acquires hyperspectral images and we used false color RGB images (wavelengths of the RGB channels: red = 590 nm; green = 530 nm; blue = 440 nm) for this study. These CRISM visible wavelengths are relatively close to the wavelength range of the CTX (500–700 nm; central wavelength 650 nm) (Malin et al., 2007) and HiRISE RED channel (570–830 nm; central wavelength 694 nm) (McEwen et al., 2007). The similarity of the filter wavelengths of the instruments, and the fact that we measured similar size distributions from the different image data sets, gives us confidence that differences in optical properties of the instruments do not affect our study.

CTX acquires 30 km wide image swaths with a spatial resolution of 6 m/pxl (Malin et al., 2007) and HiRISE 6 km wide image swaths with spatial resolutions between 0.25 and 1 m/pxl (McEwen et al., 2007). CTX images cover the whole CRISM image (image swath width of 12 km) in contrast to HiRISE. Hence, the chance to find equivalent dust devils as observed in CRISM is much more likely with CTX than with HIRISE (see also Fig. 1). In total, 14,415 images were searched to identify dust devils. It should be noted that the number of raw CRISM images was 17,709 in total, but browse images were not available for all of them. 34 CRISM browse images (0.24%) contained one or more dust devils, but only for 26 of the 34 CRISM images simultaneous CTX and/or HiRISE observations existed. It is worth to note that the orbit of MRO restricting all dust devil observations to a local mean solar time (LMST) around 1500.

Distances between the dust devil positions, diameters, shadow lengths and directions of motion were measured with the ESRI ArcGIS 9.3 software in ArcMap. The distance between the two dust devil positions were tracked from the center intersections between the dust plumes and its shadows, hence giving us the near-surface horizontal speeds (or ground speeds) of the dust devils. This measurement method is necessary as dust devils (especially taller ones with heights of a few hundred meters) are often tilted by the prevailing wind (e.g., Maxworthy, 1973), making their actual location somewhat uncertain. We consider our measurements to be precise within 3 pixels (54 and 108 m for 18 and 36 m/pxl images, respectively).

The determination of dust devil diameters and shadow lengths is not straightforward owing to their dynamic behavior and variations in morphology. Terrestrial and martian dust devils can have a

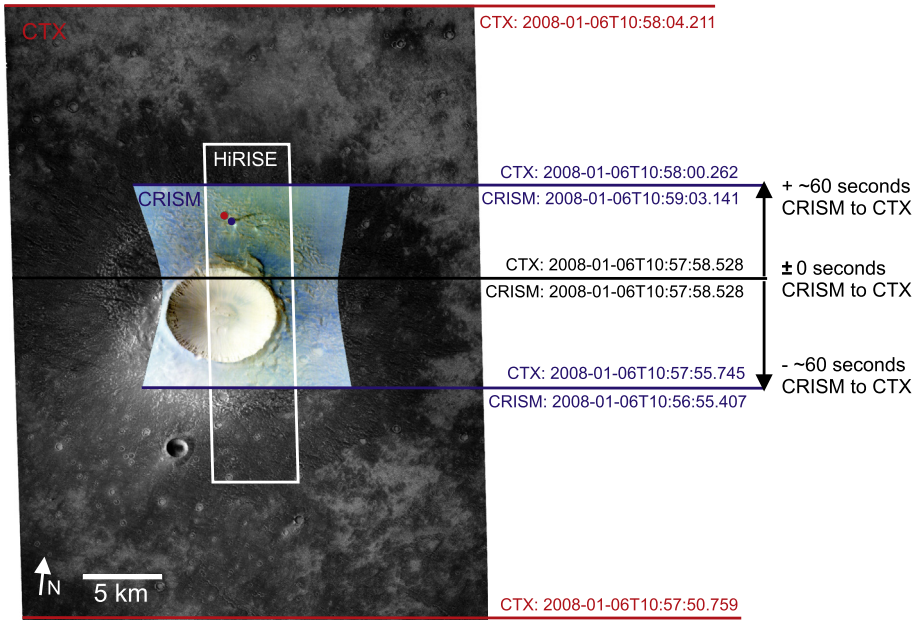

Fig. 1. Schematic illustration of CTX and CRISM with UTC imaging times of the martian surface. The time difference between CRISM and CTX in imaging the same surface area range roughly between ±1 min. HiRISE observation times (red channel) are the same as CTX imaging times. The red and blue dot indicates a dust devil observation with CTX/HiRISE and CRISM respectively in Utopia Planitia (id 4 in Table 1). In this case the 200 m in diameter dust devil was first imaged by CTX (red dot) and about 47.1 s later by CRISM (blue dot). The dust devil moved 550 m indicating a horizontal speed of 11.7 ms^{-1}. The direction of motion was to the southeast. CRISM image FRT000093B3_07_IF166S; CTX image P15_006776_2072, and HiRISE image PSP_006776_2070. (For interpretation of the references to color in this figure legend, the reader is referred to the web version of this article.)

"skirt" at the base consisting of sand and dust (Balme and Greeley, 2006; Greeley et al., 2006). These so-called sand skirts can be a few times wider than the vortex itself, leading to an overestimation of the dust devil diameter. Again, dust devils tend to be lean in the direction of motion by boundary layer winds which can also affect the exact determination of the diameter and shadow length (dust devil height). Because of these uncertainties we used conservative estimations of errors based on previous studies and visual inspections of our data. Dust devil diameters were measured in higher resolution CTX or HiRISE images. Stanzel et al. (2008) found that measurements of a dust devil in a HRSC image with a spatial resolution of 25 m/pxl is overestimated by about 50% in comparison to its size in a simultaneous acquired image by the Super Resolution Channel (SRC) (Oberst et al., 2008) with a spatial resolution of 5 m/pxl. We compared our measurements between simultaneous imaged dust devils in CTX (6 m/pxl) and HiRISE (0.25 m/pxl) images. In most cases measured dust devil diameters between both image data sets were similar (<10%), but in some cases the difference was up to 25%. We estimate the error in measuring the diameter to be <25%. Dust devil heights were measured from their shadow lengths in combination with the local solar incidence angle (measured in QView; http://isis.astrogeology.usgs.gov/IsisWorkshop/uploads/8/8b/Qview.pdf). We defined the height (top of the dust devil) as the top of the continuous column of dust, devoid of any of the discontinuities which can occur above it. Most shadow lengths are well defined, but in some cases uncertainties exist about the exact shadow lengths. Based on visual inspection during the measurement procedure, we estimate the error in measuring the shadow length to be <20%. We estimate the uncertainty in measuring the horizontal direction to be <±15°. From terrestrial dust devil observations it is known that their size, direction of motion and horizontal speed can change during their life cycle (Balme and Greeley, 2006 and references therein). Although the observation of dust devils in this study lasts at maximum ±1 min, all our measurements are averaged values based on the areographic position in the two image observations.

The horizontal motion of dust devils are compared to large-scale ambient winds extracted from the Mars Climate Database (MCD) (Lewis et al., 1999; Millour et al., 2008). MCD wind speeds are obtained by averaging LMD-GCM predictions (LMD = Laboratoire de Météorologie Dynamique) (Forget et al., 1999) over each of the twelve "months" in a martian year (each month corresponds to an interval of solar longitude of 30° at twelve fixed times of day. MCD wind fields are stored on a three-dimensional spatial grid. When data are requested at a point, it is linearly interpolated in space and time from the database grid.

MCD wind estimates only represent the contribution of average large-scale winds at a given location. This means that MCD wind fields take into account mean meridional circulations (Hadley cells), thermal tides, planetary waves, and modifications thereof by the large-scale topography. The day-to-day variability related to baroclinic wave activity is resolved by the LMD-GCM but not included in averaged MCD wind fields (it is however available as a separate diagnostic). Wind circulations triggered by the regional scale topography (e.g., Rafkin et al., 2001; Tyler et al., 2002; Spiga and Forget, 2009), unresolved at typical GCM horizontal resolutions, is not accounted for in the MCD. The fine-scale structure of baroclinic waves, namely fronts, is not included either. Hence MCD large-scale winds could depart from actual motions of dust devils in regions characterized by uneven regional topography or strong baroclinic wave activity. Furthermore, at local scales, turbulent motions in the convective boundary layer could make dust devils not following precisely the straight path imposed by large-scale and regional winds, as evidenced through in situ observations on the Earth (Balme et al., 2012) and Large-Eddy Simulations for Mars (Michaels and Rafkin, 2004). Even so, comparisons of observed dust devil horizontal motion and modeled wind fields provide an estimate of ambient wind speed and direction within the described uncertainties above for model predictions.

To compare MCD winds with observed dust devil horizontal speeds, MCD fields are extracted at the approximate altitude of the summit of the corresponding dust devils. The uncertainty on

the observed height of dust devils is used to derive an uncertainty for the retrieval of MCD wind estimates. Wind speeds are extracted from the MCD within the uncertainty range for observed dust devil heights; the resulting speed range is regarded as the uncertainty of our comparison method. This adds to the above-mentioned, intrinsic, uncertainty of MCD estimates.

3. Results

In total, 47 dust devils were identified in 26 CRISM images which have counterparts in CTX and/or HiRISE. A detailed summary is given in Table 1. Dust devil diameters range from 15 to 280 m with an average diameter of 100 m (median = 75 m). Dust devil heights range from 40 to 4400 m. Additional dust devils could be identified in CRISM data but there were no simultaneous CTX or HiRISE image acquisition. In general, most dust devils were observed in CTX imagery due to the larger areal extent the whole CRISM image covers compared to HiRISE (Fig. 1).

The global spatial distribution of the identified dust devils is shown in Fig. 2A. Dust devils occurred within a latitude range from 68.4°S to 68.3°N. 79% of the dust devils occurred in the northern and 21% in the southern hemisphere. 53% of all observed dust devils occurred in Amazonis Planitia (67.5% from the northern hemisphere dust devils). Another region with a high frequency of dust devil observations is Chryse Planitia. Four dust devils in different CRISM images were identified. Other regions of interest due to additional lander or rover observations include the Phoenix landing site (3 dust devils in one CRISM image) and the Mars Exploration Rover (MER-A) Spirit site in Gusev crater (2 dust devils in two CRISM images). A normalized distribution of dust devils per number of CRISM images and dust devils per km^2 in a 10° latitude × 10° longitude global grid is shown in Fig. 2B. In average about 20 CRISM images were acquired within 10° × 10° grid cells. In this dataset, dust devil frequencies are very low in all locations on Mars (0.01–0.1 dust devils per CRISM image or 0.0001–0.001 dust devils per km^2), except for Amazonis Planitia in two neighboring grid cells where the dust devil frequency is much higher (0.3 and 1.4 dust devils per CRISM image or 0.002–0.01 dust devils per km^2).

The majority of dust devils were observed in the northern hemisphere (79%), mainly in Amazonis Planitia (67.5% from the northern hemisphere dust devils). Fig. 3 shows the seasonal occurrence (solar longitude, L_S) of dust devils in the northern and southern hemisphere (spring equinox at $L_S = 0°$ in the northern and at $L_S = 180°$ in the southern hemisphere). In the northern hemisphere dust devils predominantly occurred in early and mid spring (76%). For the southern hemisphere no seasonal trend is found probably due to the small number of observations.

We were able to measure horizontal speeds from 44 of the 47 observed dust devils (Table 1). Two examples are shown in Fig. 4. Three horizontal speeds could not be determined because the time delay between the CRISM and CTX/HiRISE image was too short. Horizontal speeds of dust devils range from 4 to 25 ms^{-1}. The average horizontal speed of the 44 dust devils is 12 ms^{-1}. For more than two-third (73%) of the dust devils the horizontal speed is less than 15 ms^{-1}. Our dust devil sizes and horizontal speed measurements are in good agreement with previous studies as shown in Table 2. Fig. 5 shows the relationship between dust devil diameters and horizontal speeds. There is no apparent correlation between dust devil size and its horizontal speed.

We compared our measured dust devil horizontal speeds and directions to the MCD wind fields derived from GCM predictions along two different lines: (1) Comparisons with MCD wind speeds and directions at constant heights above the surface, and (2) comparisons with MCD wind speeds and directions at a height being a multiple of the dust devil top height. Detailed overviews of all our comparisons are given in Figs. S1–S4 in Supplementary material. Figs. 6 and 7 show a summary of our comparisons of dust devil horizontal speeds and directions with (1) MCD wind speeds and orientations at a constant height of 10 m above the surface (Figs. 6A and 7A), (2) MCD wind speeds and orientations at heights of 0.5 × top height of the dust devil (Figs. 6B and 7B), (3) MCD wind speeds and orientations at heights of the top height of the dust devil (Figs. 6C and 7C), and (4) MCD wind speeds and orientations at a constant height of 20 km above the surface (Figs. 6D and 7D).

The dust devil horizontal speeds are reasonably linearly correlated to MCD near surface wind speeds at 10 m above the surface, but overestimate those by a factor of approximately 2 (Fig. 6A). We find that, except for a few interesting cases, which are discussed in the next section, the dust devil horizontal speeds are generally in much better agreement with the predicted MCD horizontal wind speed within the Planetary Boundary Layer (PBL) (Fig. 6B and C, see also Figs. S1 and S2 in Supplementary material). The agreement between MCD wind speed and dust devil horizontal speed is better when we consider multiples of the actual dust devil top heights rather than constant heights above the surface for all cases. This is actually compliant with the fact that dust devils are embedded into PBL convection, and their top is linearly correlated with PBL depth. Comparisons of dust devil horizontal speeds with MCD wind speeds between 0.5 and 2 times the dust devil top height show very similar results (Fig. S1 in Supplementary material). This is somewhat in agreement with the motion of convective vortices in Large-Eddy Simulations (Toigo et al., 2003; Michaels and Rafkin, 2004; Spiga and Forget, 2009), which are "pushed" by the background wind over the whole convective PBL in which those are embedded. We also found that dust devil horizontal speeds are not in any way representative of MCD large-scale conditions more than 5 km above the surface, i.e. above the PBL top (Fig. 6D and Figs. S1 and S2 in Supplementary material).

Comparisons between dust devil directions of motion are generally in good agreement with the predicted MCD horizontal wind orientations, except for comparisons at larger heights (more than 5 km) above the surface (Fig. 7 and Figs. S3 and S4 in Supplementary material). In contrast to the comparison of near surface dust devil horizontal speeds versus MCD wind speeds, the dust devil directions of motion are in good agreement with the MCD predicted wind orientations at heights 10 m above the surface. In general our comparison shows that dust devils move in directions predetermined by wind fields within the PBL.

Our comparisons show that inferring wind speed and direction from dust devils allows for first-order estimates, but not fully accurate quantitative measurements. A conservative estimate for absolute uncertainties on PBL wind speed and direction would be respectively 5 ms^{-1} and 50°. In other words, there is a significant spread of speed and direction when comparing winds inferred from dust devils and model predictions for large-scale ambient winds. This is expected since we compare instantaneous measurements with averaged predictions from a global climate model. Large-eddy simulations show indeed that, although the horizontal motion of dust devils is governed by ambient wind (e.g., Spiga, 2012), convective vortices giving rise to dust devils are also pushed by turbulent winds (Michaels and Rafkin, 2004). The same conclusion can be drawn from Balme et al. (2012) when comparing successively dust devil wind speeds with instantaneous ambient wind speeds and with averaged wind speeds over at least a few tens of minutes.

We conclude that the dust devil horizontal speeds and direction of motion on Mars represent large-scale ambient wind conditions within the Planetary Boundary Layer (PBL). Dust devil horizontal speeds can be used as proxies for PBL wind speeds. However, dust devil horizontal speeds compared to predicted near-surface winds are significant overestimates (about a factor of 2) and could at least

Table 1
CRISM and CTX/HiRISE observations of dust devils in chronological order.

Id	Latitude	Longitude (East)	Diameter (m)	Height (m)	Direction (°)	Time interval (s)	Horizontal speed (ms^{-1})
Amazonis Planitia, 2008-01-04, L_S 12.50°, FRT000092F1_07_IF167S, P15_006747_2154							
1	35.03	200.28	50 ± 13	661 ± 132	220	52.8	11.7 ± 1.0
2	35.03	200.27	200 ± 50	397 ± 79	188	54.6	9.2 ± 1.0
Solis Planum, 2008-01-06, L_S 13.39°, FRT0000938F_07_IF163S, P15_006771_1507							
3	−29.27	273.33	60 ± 15	1204 ± 241	66	18.8	18.6 ± 2.9
Utopia Planitia, 2008-01-06, L_S 13.58, FRT000093B3_07_IF166S, P15_006776_2072, PSP_006776_2070							
4[a]	27.06	129.61	200 ± 50	1396 ± 279	122	47.1	11.7 ± 1.1
Deuteronilus Mensae, 2008-01-07, L_S 14.22°, FRT0000942B_07_IF167S, P15_006793_2292							
5	49.76	22.15	120 ± 30	918 ± 184	109	2.6	23.3 ± 21.0
Amazonis Planitia, 2008-01-15, L_S 17.89°, FRT000096FA_07_IF167S, P15_006892_2157							
6	35.27	201.28	200 ± 50	1298 ± 260	198	17.6	10.2 ± 3.1
Amazonis Planitia, 2008-01-16, L_S 18.37°, FRT00009760_07_IF167S, P15_006905_2168							
7	37.90	205.81	120 ± 30	366 ± 73	208	35.8	9.8 ± 1.5
Amazonis Planitia, 2008-01-27, L_S 23.67°, FRT00009AAB_07_IF167S, P15_007050_2169							
8	36.73	206.90	25 ± 6	701 ± 140	155	14.7	9.9 ± 3.7
9	36.69	206.85	50 ± 13	192 ± 38	126	14.5	10.3 ± 3.7
10	36.69	206.94	70 ± 18	618 ± 124	181	22.8	6.1 ± 2.4
Amazonis Planitia, 2008-01-31, L_S 25.59°, FRT00009BB9_07_IF167S, P15_007103_2153							
11	35.35	200.30	70 ± 18	597 ± 119	182	37.6	12.5 ± 1.4
12	35.26	200.28	100 ± 25	704 ± 141	198	23.8	16.4 ± 2.3
Amazonis Planitia, 2008-04-19, L_S 60.59°, FRT0000A876_07_IF167S, P18_008105_2152							
13	35.56	199.49	280 ± 70	895 ± 179	125	53.7	12.3 ± 1.0
Amazonis Planitia, 2008-04-24, L_S 62.84°, HRL0000A942_07_IF184S, P18_008171_2138, PSP_008171_2145							
14	34.32	197.57	75 ± 19	188 ± 38	87	52.4	3.8 ± 2.1
15	34.10	197.39	75 ± 19	175 ± 35	104	13.0	15.4 ± 8.3
16[a]	34.00	197.48	75 ± 19	183 ± 37	75	45.9	9.2 ± 2.4
17[a]	33.98	197.48	75 ± 19	259 ± 52	82	49.7	8.0 ± 2.2
Chyrse Planitia, 2008-04-27, L_S 64.47°, HRS0000AA17_07_IF175S, P18_008219_2054							
18	24.05	327.78	50 ± 13	134 ± 27	–	1.1	–
Amazonis Planitia, 2008-04-27, L_S 65.53°, HRL0000AA90_07_IF184S, P18_008250_2154							
19	35.38	200.13	100 ± 25	266 ± 53	94	43.8	7.2 ± 2.5
20	35.37	200.25	175 ± 44	266 ± 53	122	35.6	11.2 ± 3.0
21	35.34	200.26	80 ± 20	116 ± 23	117	28.1	8.9 ± 3.8
22	35.32	200.95	100 ± 25	619 ± 124	97	22.1	4.1 ± 4.9
23	35.27	200.35	250 ± 63	4413 ± 883	–	2.2	–
24	35.21	200.21	50 ± 13	513 ± 103	93	18.1	10.5 ± 6.0
25	35.07	200.22	200 ± 50	411 ± 82	110	55.0	7.8 ± 2.0
Meridiani Planum, 2008-10-04, L_S 135.57°, HRL0000CCF1_07_IF182S, B02_010262_1772							
26	−1.91	350.32	35 ± 9	–	45	2.8	10.7 ± 38.5
27	−1.91	350.31	40 ± 10	426 ± 85	–	0.0	–
Vastitas Borealis (Phoenix landing site), 2008-10-16, L_S 142.83°, FRT0000CF8B_07_IF168S, B02_010424_2484							
28	68.35	234.40	150 ± 38	1128 ± 226	83	58.6	13.4 ± 0.9
29	68.32	234.46	75 ± 19	583 ± 117	85	45.1	16.2 ± 1.2
30	68.30	234.14	35 ± 9	262 ± 52	112	44.1	17.3 ± 1.2
Isidis Planitia, 2009-05-20, L_S 269.73°, FRT00012C8A_07_IF165S, B09_013199_1898, ESP_013199_1900							
31[a]	10.06	83.09	100 ± 25	596 ± 119	178	54.5	14.5 ± 1.0
Gusev crater (MER-A landing site), 2009-06-13, L_S 284.31°, HRL000132F9_07_IF182S, B10_013499_1653, ESP_013499_1650							
32[a]	−14.58	175.57	15 ± 4	40 ± 8	124	22.8	25.5 ± 4.7
Sisyphi Planum, 2009-06-16, L_S 286.51°, FRT00013437_07_IF163S, B10_013545_1113, ESP_013545_1110							
33[a]	−68.61	11.43	115 ± 29	873 ± 175	118	6.2	4.8 ± 8.7
Terra Cimmeria, 2009-07-30, L_S 312.69°, HRS00013FFC_07_IF172S, B11_014107_1325							
34	−46.71	141.25	60 ± 15	56 ± 11	237	11.3	5.3 ± 9.5
Syria Planum, 2010-03-09, L_S 61.61°, FRT0001718C_07_IF164S, B19_016951_1712, ESP_016951_1710							
35[a]	−8.70	254.67	125 ± 31	1097 ± 219	29	46.7	19.5 ± 1.2
Hellas Planitia, 2010-03-14, L_S 64.06°, FRT0001737B_07_IF164S, ESP_017023_1450							
36[b]	−34.73	92.12	75 ± 19	1110 ± 222	30	40.1	17.0 ± 1.3
Chyrse Planitia, 2010-05-16, L_S 91.67°, FRT00018D3C_07_IF166S, ESP_017832_2065							
37[b]	26.33	315.58	50 ± 13	212 ± 42	129	19.0	6.1 ± 2.8
Xanthe Terra, 2011-03-27, L_S 262.43, FRT0001D806_07_IF165S, G09_021867_1902, ESP_021867_1900							
38[a]	9.73	316.07	200 ± 50	857 ± 171	183	49.4	20.2 ± 1.1
Gusev crater (MER-A landing site), 2011-03-31, L_S 265.28°, FRT0001D8DC_07_IF124S, G09_021925_1653, ESP_021925_1650							
39[a]	−14.66	175.54	50 ± 25	130 ± 26	120	34.2	12.1 ± 1.6
Chyrse Planitia, 2011-04-30, L_S 283.66°, FRT0001DF63_07_IF126S, G10_022302_1949, ESP_022302_1950							
40[a]	14.78	320.78	100 ± 25	1433 ± 287	189	24.4	16.8 ± 2.2

Table 1 (*continued*)

Id	Latitude	Longitude (East)	Diameter (m)	Height (m)	Direction (°)	Time interval (s)	Horizontal speed (ms^{-1})
Solis Planum, 2011-05-06, L_S 287.54°, FRT0001E121_07_IF124S, G11_022383_1557							
41	−24.22	273.73	25 ± 6	–	135	19.2	10.4 ± 2.8
Chyrse Planitia, 2011-05-17, L_S 294.34°, FRT0001E2AB_07_IF166S, G11_022526_2141							
42	33.91	321.78	75 ± 19	–	78	20.3	14.0 ± 2.7
Terra Sabea/Syrtis Major Planum, 2011-06-20, L_S 314.21°, FRT0001EAE0_07_IF166S, G12_022957_1985							
43	18.46	77.54	100 ± 25	398 ± 80	252	49.9	6.2 ± 1.1
Amazonis Planitia, 2011-11-25, L_S 34.46°, FRT00021845_07_IF127S, G17_024983_2155, ESP_024983_2160							
44	35.53	202.10	70 ± 18	178 ± 36	138	18.7	11.8 ± 2.9
45[a]	35.52	202.02	140 ± 35	542 ± 108	134	17.0	17.6 ± 3.2
46[a]	35.49	202.05	150 ± 38	324 ± 65	150	3.3	9.1 ± 16.4
47	35.45	202.11	180 ± 45	552 ± 110	125	34.4	12.5 ± 1.6

[a] These dust devils were additionally to CTX imaged by HiRISE.
[b] These dust devils were only imaged by HiRISE, not by CTX. A more detailed table is available in Fig. S5 in Supplementary material.

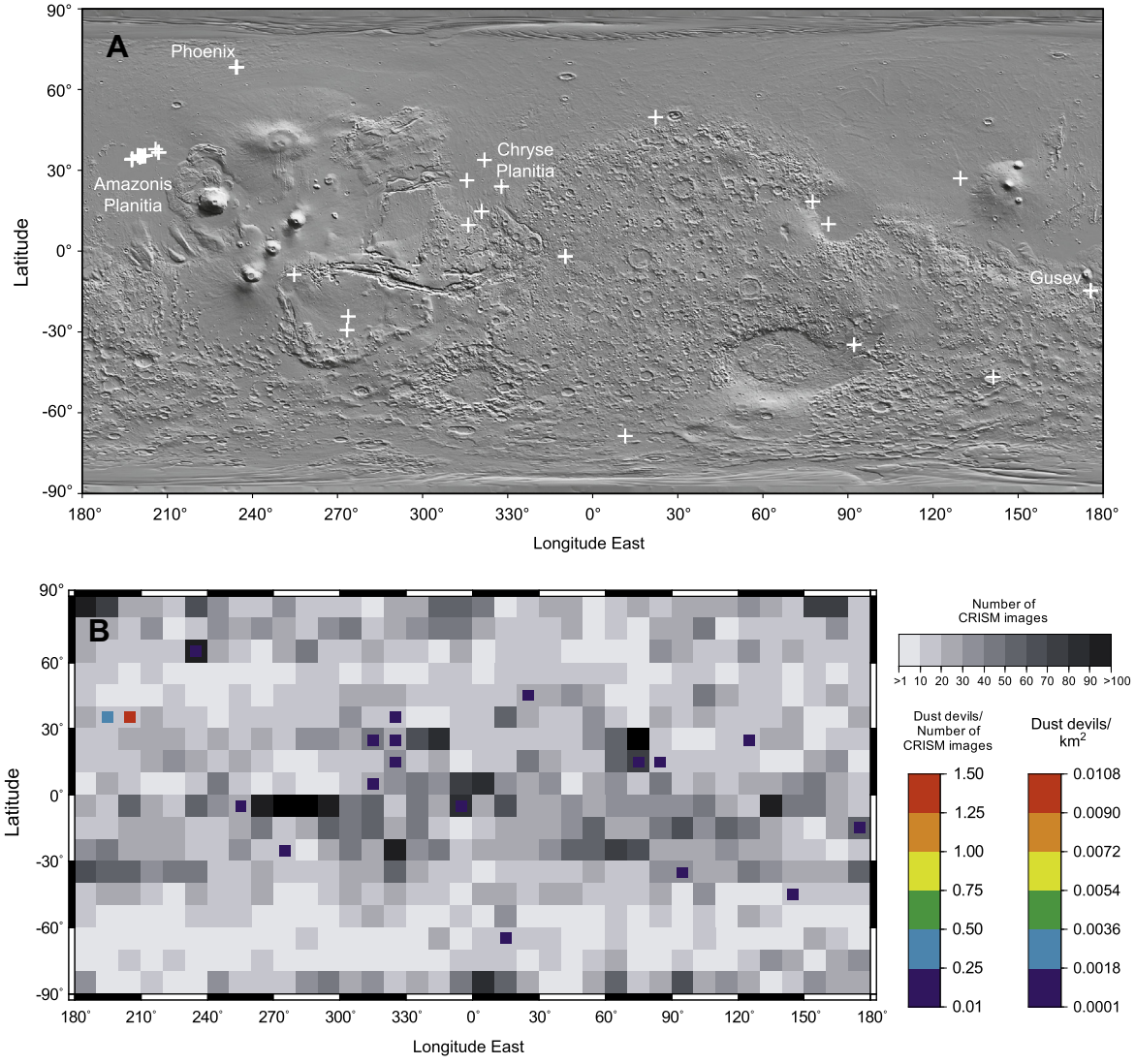

Fig. 2. (A) Simple cylindrical shaded relief (Mars Orbiter Laser Altimeter (MOLA) topography) with the global distribution of individual dust devils (see Table 1). (B) Normalized distribution of dust devils per number of CRISM images and dust devils per km^2 in a 10° latitude × 10° longitude global grid. Number of CRISM images per grid cell is shown in grayscale. Smaller colorized squares within the grid cells indicate the dust devil frequency (dust devils per number of CRISM images). (For interpretation of the references to color in this figure legend, the reader is referred to the web version of this article.)

only be considered as rough proxies for near-surface winds. In contrast, dust devil directions of motion can be used as proxies for near surface wind orientations. Dust devil horizontal speeds and directions cannot represent good estimates for wind fields a few kilometers above the PBL top.

Some dust devil horizontal speeds (id 28–30, and 32 in Fig. 6) and horizontal directions (id 28–30 in Fig. 7) show a very large off-

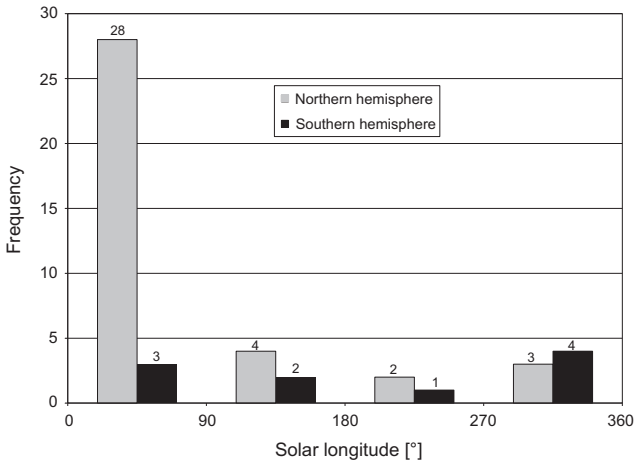

Fig. 3. Seasonal frequencies of dust devils in the northern and southern hemisphere. Seasons are given in solar longitude (L_S). Spring equinox at $L_S = 0°$ in the northern hemisphere and at $L_S = 180°$ in the southern hemisphere.

set to the MCD wind speed and wind orientation predictions at times the dust devils occurred. This cannot be explained simply by the spread induced by turbulent motions in the boundary layer as discussed in the previous paragraph. Instead, those cases where winds inferred from dust devils differ completely from predicted GCM winds, point towards regional, meteorological processes not resolved in the GCM. These dust devils occurred near the Phoenix landing site (id 28–30) and at Gusev crater (id 32) which allows us to confront the disagreement between dust devil horizontal motion and predicted wind fields with lander/rover observations, and offer a more detailed discussion in what follows.

3.1. Gusev crater

The horizontal directions for the two Gusev crater dust devils are consistent with the ambient horizontal wind speed direction derived from LMD-GCM model predictions. One dust devil occurred in late spring (id 39; $L_S = 265°$) (Fig. 8), the other one in early summer (id 32; $L_S = 285°$) (Fig. 9). The observed horizontal directions are also in broad agreement with observed dust devil horizontal directions based on the sequential imaging by Greeley

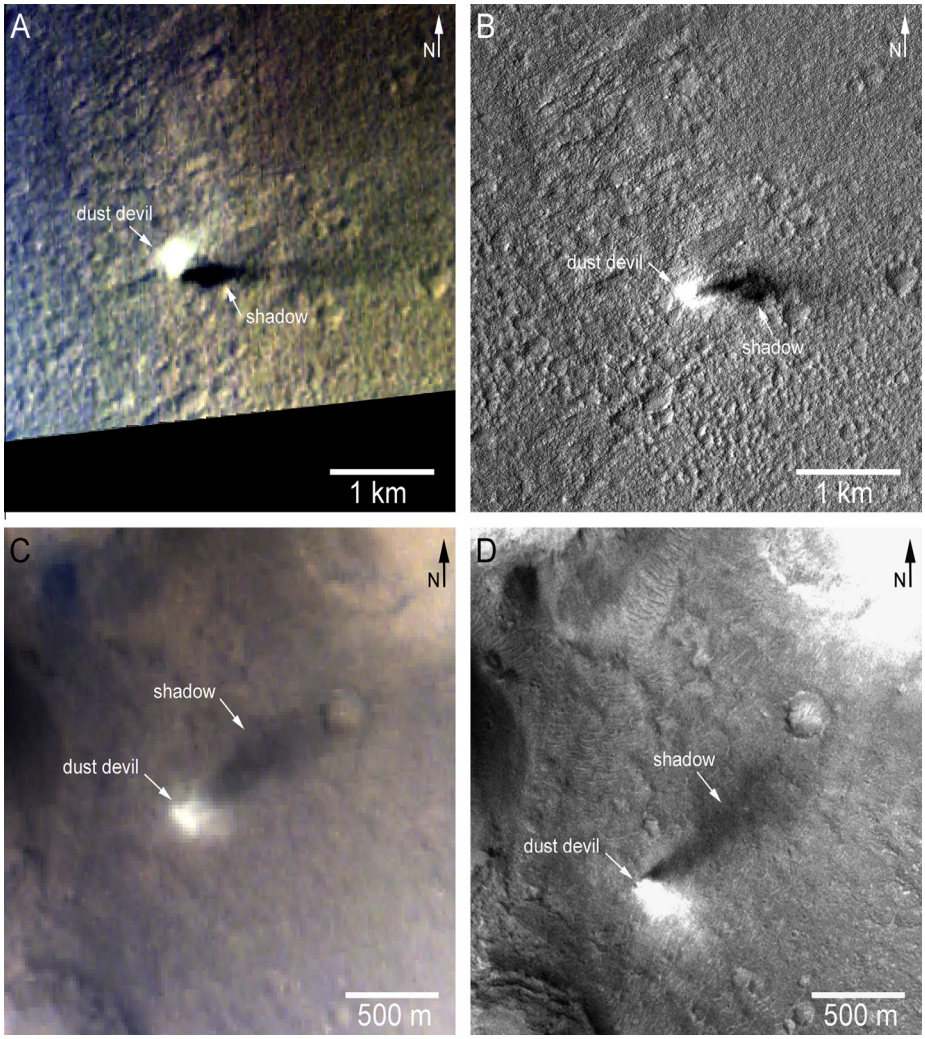

Fig. 4. Examples of identical dust devils imaged by CRISM and CTX. (A) CRISM image FRT0000A876_07_IF167S with a 280 m in diameter dust devil. (B) The same dust devil as observed in (A) imaged by CTX (P18_008105_2152) 53.67 s later. The dust devil moved 660 m between the CRISM and CTX observation indicating a horizontal speed of 12.3 ms^{-1}. The dust devil moved in southeast direction (id 13 in Table 1). (C) CRISM image FRT0001DF63_07_IF126S with a 100 m in diameter dust devil. (D) The same dust devil as observed in (C) imaged by CTX (G10_022302_1949) 24.38 s later. The dust devil moved 410 m between the CRISM and CTX observation indicating a horizontal speed of 16.8 ms^{-1}. The dust devil moved in south direction (id 40 in Table 1).

Table 2
Comparison of dust devil diameter, height and horizontal speed ranges with previous studies.

	This study	Stanzel et al. (2008)	Reiss et al. (2011b)	Greeley et al. (2010)
Number of dust devils[a]	44	205	26	498
Diameter (m)	15–280	45–1650	50–850	2–275
Height (m)	40–4400	75–4440	65–1685	10–360[b]
Horizontal speed (ms^{-1})	4–25	1–59	3–22	1–27

[a] Number of dust devils refer to horizontal speed measurements.
[b] These height ranges are taken from Greeley et al. (2006).

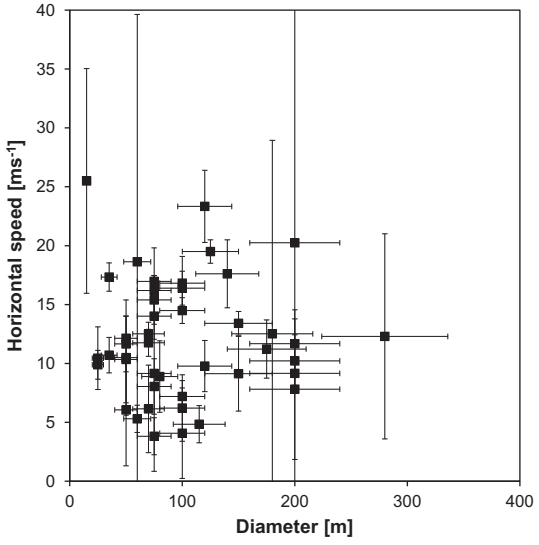

Fig. 5. Dust devil horizontal speeds as function of dust devil diameter.

et al. (2006). In spring, dust devil horizontal directions tend toward the northeast, but the direction of the strongest winds is toward the southeast (Greeley et al., 2006) consistent with the relatively fast dust devil we observed (id 39; 12.1 ms^{-1}) which moves in southeast direction (120°). In summer the observed prevailing wind direction is to the southeast (Greeley et al., 2006) also in agreement to our other dust devil measurement (id 32; 124°).

One dust devil horizontal speed (id 39; 12.1 ms^{-1}) is consistent with LMD-GCM ambient modeled wind speeds (12.4 ms^{-1}). However, the horizontal speed of one dust devil (id 32; 25.5 ms^{-1}) does not agree with the MCD ambient wind speed. The comparison of our two measured Gusev crater horizontal speeds with surface observations by Greeley et al. (2006, 2010) is also less clear. A large dataset of dust devil horizontal speeds was derived from MER-A (Spirit) image sequences at Gusev crater (Greeley et al., 2006, 2010). The horizontal speeds range between 0.1 and 27 ms^{-1} (n = 498), but the median speeds with around 2 ms^{-1} are relatively low (Greeley et al., 2010). Interestingly, our two horizontal speeds of 12.1 and 25.5 ms^{-1} are within the range of the much larger surface dataset, but definitely in the upper limit where only few horizontal speeds (2.2%) are >10 ms^{-1} (Greeley et al., 2010). Due to our limited dataset from Gusev crater it is difficult to determine if our high horizontal speeds are coincidental compared to the mean values of Greeley et al. (2010). Although the dataset contains much smaller dust devil diameters than normally observed from orbit (better resolution by the rover camera and/or regional differences in dust devil populations), both of our dust devils have comparable diameters (15 m and 50 m) well within the range of many diameters of Greeley et al. (2010), hence the dust devil diameter should have no effect. Another explanation could be the different measurement techniques. Greeley et al. (2006, 2010) calculated horizontal speeds based on the framing rate of sequential images with one camera and 2–4 landmarks to define the position between the images. However, the average horizontal speeds derived by Greeley et al. (2010) are in relatively good agreement with measurements on Earth. The largest dataset from two different regions in southwestern USA is provided by Balme et al. (2012). The horizontal speeds are in a range of 0.1–20 ms^{-1}, but daily mean values range from 2 to 12 ms^{-1} for one region and 2 to 9 ms^{-1} for another region with a large scattering between different days (Balme et al., 2012). As shown by Balme et al. (2012) this is just an effect of changing daily ambient wind speeds. Interestingly, Greeley et al. (2006) pointed out based on Mars Regional Atmospheric Modeling System (MRAMS) (Rafkin et al., 2001; Rafkin and Michaels, 2003) that ambient wind of 1–3 ms^{-1} at a height of 2 m occurred during noon which is in agreement with the dust devil horizontal speeds observed in Gusev crater. However, wind speed increases late in the day and most of the dust devils with horizontal speeds >2 ms^{-1} occurred after 1300 local mean solar time (LMST) (Greeley et al., 2006) and are in broad agreement with our LMD-GCM model predictions and observed horizontal speeds both occurring at 1500 LMST.

In summary, our measured horizontal speeds in Gusev crater are in good agreement (except for one horizontal speed) with the LMD-GCM model predictions for ambient wind fields within the PBL. In comparison with dust devil surface observations by Greeley et al. (2006, 2010) our horizontal direction measurements are consistent. One dust devil horizontal speed is relatively fast compared to most measured dust devil horizontal speeds from the surface (Greeley et al., 2006, 2010), but remains in the range of the surface measurements.

3.2. Phoenix landing site

Three active dust devils were observed about 2.5 km north the Phoenix landing site (Fig. 10). At the observation time of CRISM/CTX on 2008-10-16 (L_S = 142.83°) the Phoenix lander was still active. This allows us to compare our results with lander observations. Especially, wind speed and direction measurements (Holstein-Rathlou et al., 2010) and detected dust devil encounters from pressure drops (Ellehoj et al., 2010) are available. Our measured dust devil horizontal speeds and directions (id 28, 29, and 30) near the Phoenix landing site are those showing the largest offset compared to the LMD-GCM wind speed and direction model predictions. The comparison of our orbital dust devil measurements from the Phoenix landing site with detailed surface observations measured by Phoenix landing site instruments allows us to assess why we do have so large offsets in contrast to our generally consistent results in other areas on Mars.

The three dust devils observed by CRISM and CTX occurred at L_S = 142.83° and moved with a horizontal speed of 15 ms^{-1} in an eastward direction. The LMD-GCM model predicts relatively low wind speeds with 2 ms^{-1} in westward direction, which disagrees with our dust devil horizontal speed measurements.

At the Phoenix landing site average daytime wind speeds until L_S = 123° were generally around 4 ms^{-1} (Holstein-Rathlou et al., 2010) in a westward direction with a 360° rotation during midday. Increased wind speeds occurred at L_S = 112° and L_S = 120° correlating with increased dust devil activity (Ellehoj et al., 2010). From L_S = 127–148° a steady increase in daytime average wind speeds of 6–10 ms^{-1} generally in an eastward direction were observed

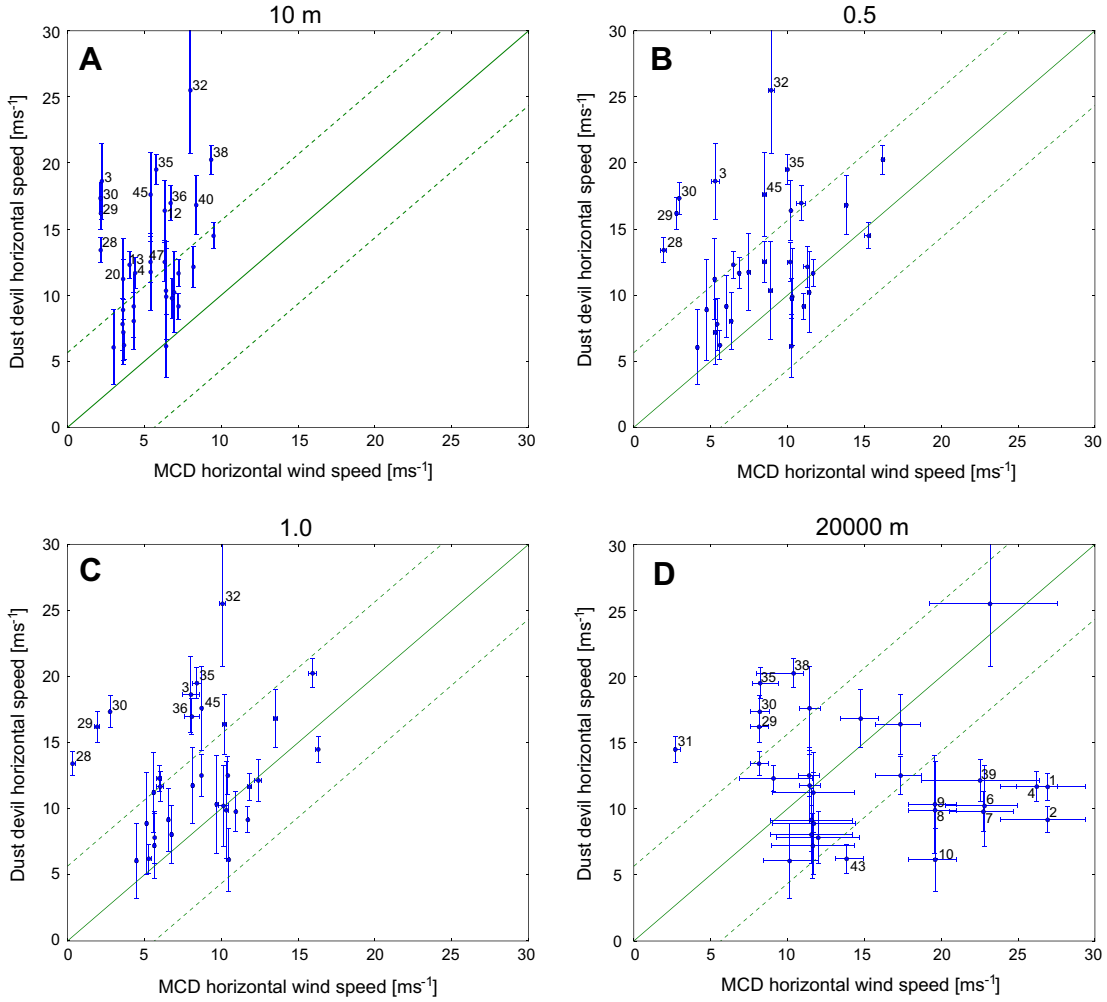

Fig. 6. (A) Dust devil horizontal speeds versus MCD horizontal wind speeds at a constant height of 10 m above the surface. (B) Dust devil horizontal speeds versus MCD horizontal wind speeds at a multiple dust devil top height of 0.5. (C) Dust devil horizontal speeds versus MCD horizontal wind speeds at heights of the dust devil top height (multiple height of 1.0). (D) Dust devil horizontal speeds versus MCD horizontal wind speeds at a constant height of 20 km above the surface. Numbers equal the individual dust devil Id in Table 1.

with a maximum wind speed of 16 ms^{-1} at $L_S = 147°$ (Holstein-Rathlou et al., 2010). Increased dust devil activity in this time period was observed at $L_S = 137°$ and $L_S = 148°$ (Ellehoj et al., 2010).

Our measured dust devil horizontal speeds and directions are in very good agreement with landing site observations showing relatively high wind speeds in an eastward direction during the same time period. Based on mapping of dust devil tracks and wind streaks from orbital datasets Holstein-Rathlou et al. (2010) found a predominant a westward or an eastward wind direction and suggested that dust devils more likely move in an eastward direction due to the wind direction measurements after $L_S = 120°$. In addition, Ellehoj et al. (2010) surveyed the Surface Stereo Imager (SSI) dataset mounted on the Phoenix lander for active dust devil passages. A total of 76 active dust devils were detected during $L_S = 125–142°$ (Ellehoj et al., 2010). Although it was difficult to determine the exact direction of motion for these dust devils due to the lack of clear landmarks the most likely direction of motion was suggested to be in an eastward (Ellehoj et al., 2010). Our measurements show that all three dust devils moved in an eastward direction, which is in agreement with the suggested travel directions of other dust devils observed during the same time period at the Phoenix landing site (Ellehoj et al., 2010; Holstein-Rathlou et al., 2010). However, although this agreement does not imply that all dust devils within the Phoenix landing site area traveled in an eastward direction, it indicates a preferred eastward travel direction of dust devils with the prevailing ambient wind fields during this time period.

Orbital and lander data show evidence for passing weather systems consisting of condensate clouds over the Phoenix landing site after $L_S = 111°$ and within the time period of our dust devil occurrences around $L_S = 143°$ (Holstein-Rathlou et al., 2010; Ellehoj et al., 2010; Moores et al., 2010). These condensate clouds passing over the landing site are probably caused by dust storm activity in the north polar region. Orbital data shows starting dust storm activity in the north polar region around $L_S = 137°$, which spread out at L_S 138°, and lead to a major dust storm centered at 76°N and 143°E at L_S 138° (Holstein-Rathlou et al., 2010). Interestingly, probable condensate clouds associated with the three observed dust devils can be identified in the CRISM image at $L_S = 142.83°$ (Fig. 10B). The disagreement between our measured dust devil horizontal speeds and directions with the LMD-GCM model predictions could therefore be explained by a front passing over the Phoenix landing site (perhaps the prelude of a flushing dust storm). An analysis of surface pressure day-to-day variability in the LMD-GCM shows indeed that baroclinic activity at the Phoenix location is significant (several Pa s^{-1}) from $L_S = 130°$ (late northern summer) to early northern spring, with peaking activity in northern winter. A front passing over the Phoenix landing site at $L_S = 143°$

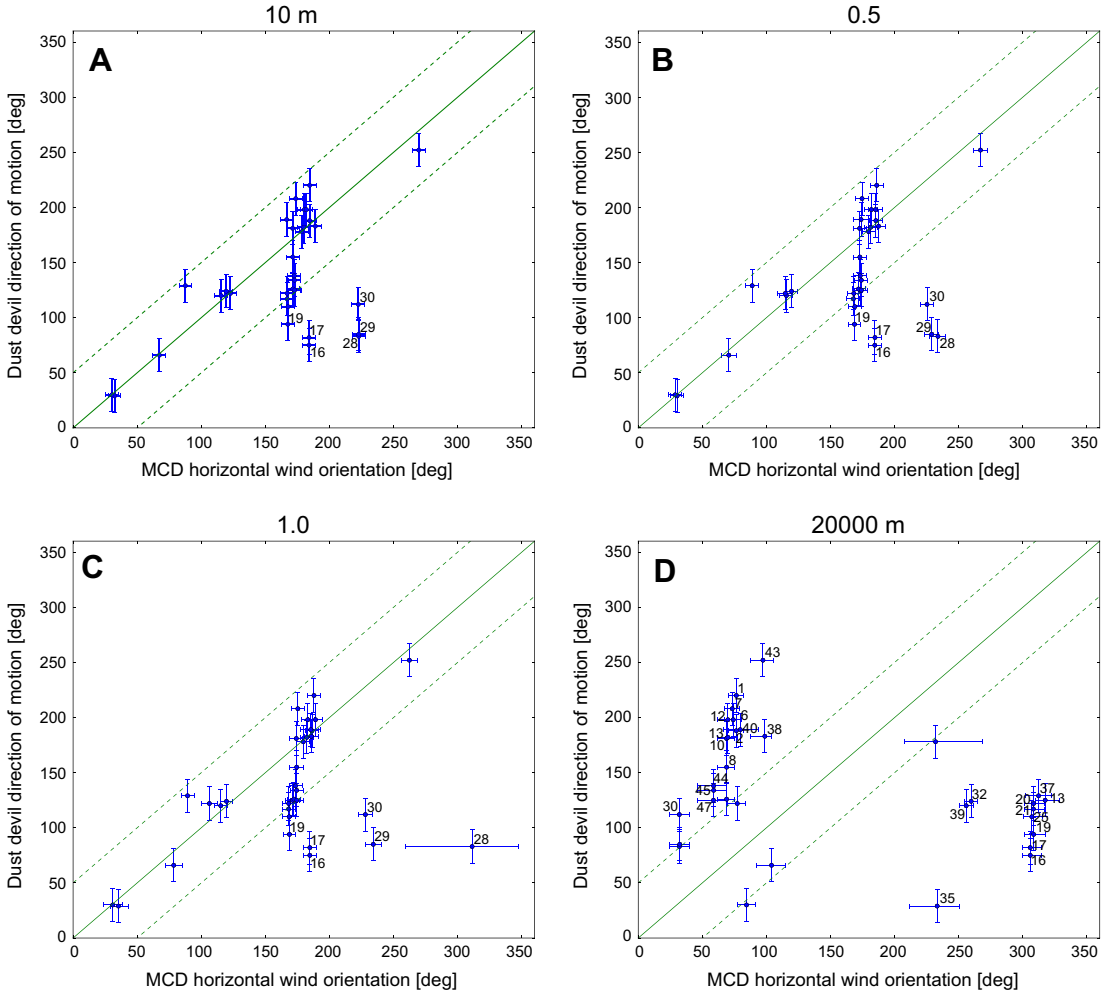

Fig. 7. (A) Dust devil directions of motion versus MCD horizontal wind orientations at a constant height of 10 m above the surface. (B) Dust devil directions of motion versus MCD horizontal wind orientations at a multiple dust devil top height of 0.5. (C) Dust devil directions of motion versus MCD horizontal wind orientations at heights of the dust devil top height (multiple height of 1.0). (D) Dust devil directions of motion versus MCD horizontal wind orientations at a constant height of 20 km above the surface. Numbers equal the individual dust devil Id in Table 1.

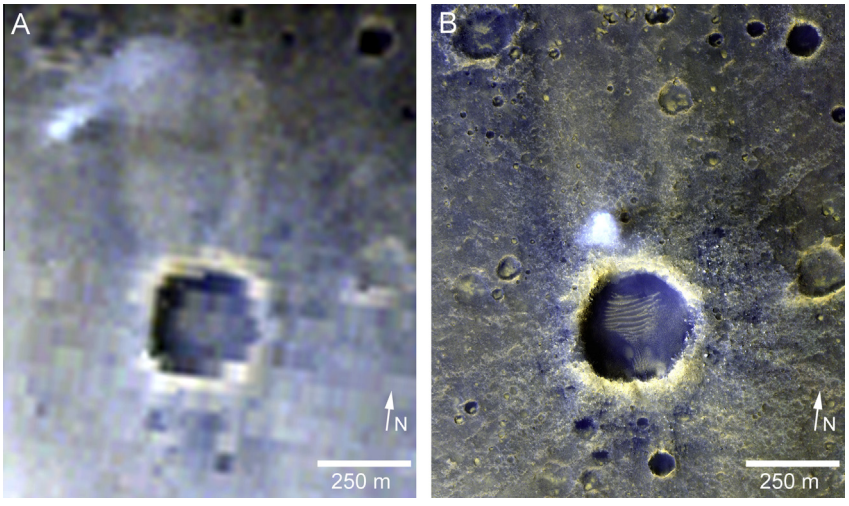

Fig. 8. (A) CRISM image FRT0001D8DC_07_IF124S with a 50 m in diameter dust devil. (B) The same dust devil as observed in (A) imaged by HiRISE (ESP_021925_1650) 34.2 s later. The dust devil moved 415 m between the CRISM and HiRISE observation indicating a horizontal speed of 12.1 ± 1.6 ms^{-1}. The dust devil moved in southeast direction (id 39 in Table 1).

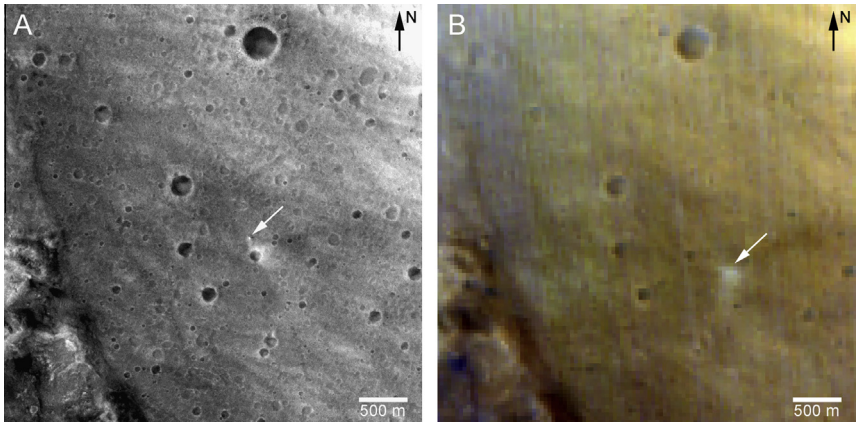

Fig. 9. (A) CRISM image CTX image B10_013499_1653 with a 15 m in diameter dust devil (white arrow). (B) The same dust devil (white arrow) as observed in (A) imaged by CRISM (HRL000132F9_07_IF182S) 22.8 s later. The dust devil moved 580 m between the CTX and CRISM observation indicating a horizontal speed of 25.5 ± 4.7 ms^{-1}. The dust devil moved in southeast direction (id 32 in Table 1).

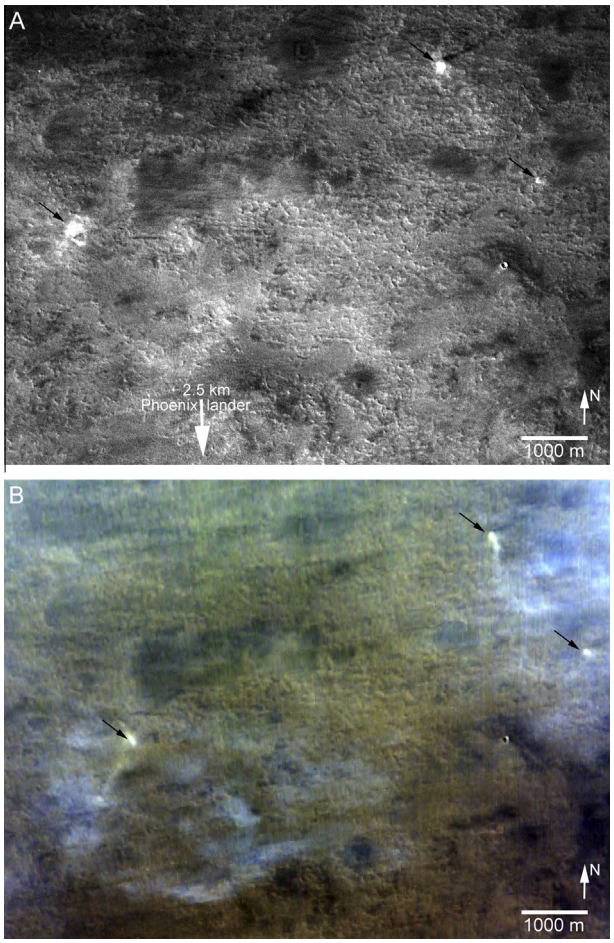

Fig. 10. Dust devils observed near the Phoenix landing site. (A) CTX image B02_010424_2484 with three dust devils (black arrows). (B) The same dust devils as observed in (A) imaged by CRISM (FRT0000CF8B_07_IF168S) 44–59 s later (black arrows). The dust devils moved with a horizontal speed of 15 ms^{-1} to the east. Note the bright, white-bluish (water ice?) clouds in the CRISM image. The CRISM and CTX images were acquired on 2008-10-16 at L_S 142.83°. At this date the Phoenix lander located about 2.5 km south of the images was still operating. (For interpretation of the references to color in this figure legend, the reader is referred to the web version of this article.)

would not be the most severe event witnessed during a martian year in those regions, but would be significant enough for measured ambient winds to clearly depart from monthly climatologies.

4. Discussion

On a global scale our observed dust devil distribution is similar to previous global studies. Highest abundances were found in Amazonis and Chryse Planitia which is in agreement with previous observations (Fisher et al., 2005; Cantor et al., 2006; Stanzel et al., 2008). Based on previous observations Amazonis Planitia seems to be in general a region of high dust devil frequency (Fisher et al., 2005; Cantor et al., 2006), although Stanzel et al. (2008) found no increased dust devil activity in Amazonis Planitia. Our normalized dust devil frequencies support the studies of Fisher et al. (2005) and Cantor et al. (2006) that Amazonis Planitia is a region of unusual high dust devil frequency on Mars. In Chryse Planitia, Stanzel et al. (2008) detected many active dust devils in southern Chryse Planitia in contrast to Fisher et al. (2005) and Cantor et al. (2006) who observed a relatively low dust devil frequency. Our normalized dust devil frequencies support the studies of Fisher et al. (2005) and Cantor et al. (2006) that Chryse Planitia is not a region of unusual high dust devil frequency on Mars. The lack of dust devil observations between 50°S and 60°S in our study (only one dust devil was detected) is in contrast to the observations by Cantor et al. (2006) and Stanzel et al. (2008). One reason might be fewer image acquisitions by CRISM (see also Fig. 2B) due to spectrally less interesting regions mainly composed of relatively smooth and dust covered highland terrains.

Early studies showed that dust devils are most common in spring and summer when insolation reaches its maximum (Ryan and Lucich, 1983; Thomas and Gierasch, 1985). This is expected because dust devil formation is associated with atmospheric daytime PBL convection controlled by instability above a warm surface (e.g., Balme and Greeley, 2006). Significant statistical data to compare the seasonal occurrence of our observed dust devils to previous studies exist only for the northern hemisphere. The high dust devil activity in early and mid spring in the northern hemisphere is in good agreement with previous studies of Stanzel et al. (2008) and Greeley et al. (2010) which observed dust devil peak frequencies in spring, whereas Cantor et al. (2006) reported dust devil peak activities during midsummer in both hemispheres. Peak activities of dust devils in Amazonis Planitia were also observed during spring (Fisher et al., 2005) in agreement with our results.

Based on theoretical modeling it was suggested that stronger ambient winds lead to larger dust devils (Rennó et al., 1998). We found no correlation between dust devil diameter and its horizontal speeds consistent with previous studies on Mars using satellite data (Stanzel et al., 2006, 2008; Reiss et al., 2011b) and surface

measurements on Earth (Balme et al., 2012). Interestingly, Greeley et al. (2010) reports that data obtained through surface observations in Gusev crater on Mars show a trend that smaller dust devils seem to move faster across the surface, but the authors also note that there is a substantial scattering in the data for all three investigated seasons.

Our measured dust devil horizontal speeds are in good agreement with previous measurements on Mars derived from satellite data. They range between 4 and 25 ms^{-1} ($n = 44$) which is well within the range between 1 and 59 ms^{-1} ($n = 205$) measured by Stanzel et al. (2008) using HRSC data on a global scale. They are also in good agreement with measurements done by Reiss et al. (2011b) with a range between 3 and 22 ms^{-1} ($n = 26$) using HRSC data on a regional scale. Average dust devil horizontal speeds of 12 ms^{-1} (median = 11.5 ms^{-1}) are consistent with average horizontal speeds of 12 ms^{-1} measured by Reiss et al. (2011b), but much lower than the average horizontal speeds of 23 ms^{-1} derived by Stanzel et al. (2008). However, as noted by Stanzel et al. (2008) the majority of these dust devils have a horizontal speed lower than 15 ms^{-1} which is in agreement with our results that 73% of the dust devils have horizontal speeds <15 ms^{-1}.

The measured horizontal speeds and directions of the dust devils are in broad agreement with the LMD-GCM wind speed and wind orientation predictions within the PBL at times the dust devils occurred although there is a spread of the data. The standard deviation for a reference case at the dust devil top height (multiple height of 1) is 4.5 ms^{-1} based on a linear fit to the cloud of points. Discrepancies could be due to (1) Dust devils are moved by large-scale winds, regional winds and turbulent convective cells. The latter probably account for the spread of the data when instantaneous winds given by dust devils are compared against large-scale winds predicted by GCMs (or even regional winds predicted by mesoscale models). (2) Dust devils were observed when a meteorological front was passing in the considered region, which is not captured in the MCD average wind fields used for comparisons, but rather in the day-to-day variability products of the database. (3) Local topography and thermal wind generated by contrasts in soil properties (e.g. albedo, thermal inertia, ice cover versus bare soil) could give rise to regional or local wind regimes left unresolved by GCMs.

Our results show that dust devils on Mars move with ambient wind fields confirming previous studies on Mars (Stanzel et al., 2006, 2008) and Earth (e.g., Balme et al., 2012). They also indicate that dust devils on Mars move with horizontal speeds which equal boundary layer wind speeds, hence faster than near surface winds in agreement with terrestrial results (Balme et al., 2012). Horizontal speeds of our measured dust devils are about a factor of 2 faster than the MCD predicted near surface winds at a height of 10 m above the surface. Interestingly, Balme et al. (2012) noticed the same trend that dust devils moved 10–20% faster than ambient wind speeds measured at 10 m height above ground level. Balme et al. (2012) calculated the height above the surface where dust devil horizontal speeds are equivalent to ambient winds within the PBL (about 20–30 m above the surface). They emphasized that this does not mean that dust devil speeds are only influenced by the wind at one height but reflecting "both an integrated wind profile over its whole cross-section and the integrated effect of the frictional near-surface boundary layer" (Balme et al., 2012). In contrast, our martian results indicate a much larger (about an factor of 2) offset between measured dust devil horizontal speeds and MCD near-surface wind speed predications at 10 m height above the surface. Despite the uncertainties in our comparisons discussed above, there might be several other reasons for our conclusions to differ from Balme et al. (2012) results: differences in the PBL and surface layer between Earth and Mars, differences of dust devil sizes analyzed in the two studies, and differences in analysis techniques (in situ studies versus remote sensing and model results). However, our new introduced method for measuring horizontal speeds and directions of dust devils with MRO instruments offers future perspectives to better understand dust devil processes on Mars, using, e.g., near-surface wind speed measurements at the current Mars Science Laboratory (MSL) landing site in Gale crater.

Acknowledgments

This research has made use of the USGS Integrated Software for Imagers and Spectometers (ISIS). We would like to thank two anonymous reviewers for their constructive and helpful reviews which improved an earlier version of the manuscript.

Appendix A. Supplementary material

Supplementary data associated with this article can be found, in the online version, at http://dx.doi.org/10.1016/j.icarus.2013.08.028.

References

Balme, M., Greeley, R., 2006. Dust devils on Earth and Mars. Rev. Geophys. 44, RG3003. http://dx.doi.org/10.1029/2005RG000188.

Balme, M.R., Pathare, A., Metzger, S.M., Towner, M.C., Lewis, S.R., Spiga, A., Fenton, L., Renno, N.O., Elliott, H.M., Saca, F.a., Michaels, T., Russell, P., Verdasca, J., 2012. Field measurements of horizontal forward motion speeds of terrestrial dust devils: Towards a proxy for ambient winds on Mars and Earth. Icarus 221, 632–645.

Cantor, B.A., Kanak, K.M., Edgett, K.S., 2006. Mars Orbiter Camera observations of martian dust devils and their tracks (September 1997 to January 2006) and evaluation of theoretical vortex models. J. Geophys. Res. 111, E12002. http://dx.doi.org/10.1029/2006JE002700.

Choi, D.S., Dundas, C.M., 2011. Measurements of martian dust devil winds with HiRISE. Geophys. Res. Lett. 38, L24206. http://dx.doi.org/10.1029/2011GL049806.

Crozier, W.D., 1970. Dust devil properties. J. Geophys. Res. 75, 4583–4585.

Ellehoj, M.D. et al., 2010. Convective vortices and dust devils at the Phoenix Mars mission landing site. J. Geophys. Res. 115, E00E16. http://dx.doi.org/10.1029/2009JE003413.

Exelis Visual Information Solutions, 2013. ENVI Tutorials, April 2013. <http://www.exelisvis.com/Learn/Resources/Tutorials.aspx>.

Fisher, J.A. et al., 2005. A survey of martian dust devil activity using Mars Global Surveyor Mars Orbiter Camera images. J. Geophys. Res. 110, E03004. http://dx.doi.org/10.1029/2003JE002165.

Flower, W.D., 1936. Sand devils. Lond. Meteorol. Off. Prof. Notes 5, 1–16.

Forget, F. et al., 1999. Improved General Circulation Models of the martian atmosphere from the surface to above 80 km. J. Geophys. Res. 104, 24155–24175.

Greeley, R. et al., 2005. Martian variable features: New insight from the Mars Express Orbiter and the Mars Exploration Rover Spirit. J. Geophys. Res. 110, E06002. http://dx.doi.org/10.1029/2005JE002403.

Greeley, R. et al., 2006. Active dust devils in Gusev crater, Mars: Observations from the Mars Exploration Rover Spirit. J. Geophys. Res. 111, E12S09. http://dx.doi.org/10.1029/2006JE002743.

Greeley, R. et al., 2010. Gusev crater, Mars: Observations of three dust devil seasons. J. Geophys. Res. 115. http://dx.doi.org/10.1029/2010JE003608.

Holstein-Rathlou, C. et al., 2010. Winds at the Phoenix landing site. J. Geophys. Res. 115, E00E18. http://dx.doi.org/10.1029/2009JE003411.

Lewis, S.R. et al., 1999. A climate database for Mars. J. Geophys. Res. 104, 24177–24194.

Malin, M.C., Edgett, K.S., 2001. Mars Global Surveyor Mars orbiter Camera: Interplanetary cruise through primary mission. Journal of Geophysical Research 106, 23429–23570.

Malin, M.C. et al., 2007. Context Camera Investigation on board the Mars Reconnaissance Orbiter. J. Geophys. Res. 112, E05S04. http://dx.doi.org/10.1029/2006JE002808.

Maxworthy, T., 1973. A vorticity source for large-scale dust devils and other comments on naturally occurring columnar vortices. J. Atmos. Sci. 30, 1717–1722.

McEwen, A.S. et al., 2007. Mars Reconnaissance Orbiter's High Resolution Imaging Science Experiment (HiRISE). J. Geophys. Res. 112, E05S02. http://dx.doi.org/10.1029/2005JE002605.

Metzger, S.M., Carr, J.R., Johnson, J.R., Parker, T.J., Lemmon, M.T., 1999. Dust devil vortices seen by the Mars Pathfinder camera. Geophys. Res. Lett. 26, 2781–2784.

Michaels, T.I., Rafkin, S.C.R., 2004. Large-eddy simulation of atmospheric convection on Mars. Q. J. R. Meteorol. Soc. 130, 1251–1274.

Millour, E. et al., 2008. The latest (version 4.3) Mars Climate Database. In: Third International Workshop on the Mars Atmosphere: Modeling and Observations,

held November 10–13, 2008 in Williamsburg, Virginia. LPI Contribution No. 1447. Abstract #9029.
Moores, J.E., Lemmon, M.T., Smith, P.H., Komguem, L., Whiteway, J. A., 2010. Atmospheric dynamics at the Phoenix landing site as seen by the Surface Stereo Imager. Journal of Geophysical Research 115, E00E08. http://dx.doi.org/10.1029/2009JE003409.
Murchie, S. et al., 2007. Compact Reconnaissance Imaging Spectrometer for Mars (CRISM) on Mars Reconnaissance Orbiter (MRO). J. Geophys. Res. 112, E05S03. http://dx.doi.org/10.1029/2006JE002682.
Newman, C.E., Lewis, S.R., Read, P.L., Forget, F., 2002. Modeling the martian dust cycle, 1. Representations of dust transport processes. J. Geophys. Res. 107, 5123. http://dx.doi.org/10.1029/2002JE001910.
Oberst, J. et al., 2008. The imaging performance of the SRC on Mars Express. Planet. Space Sci. 56, 473–491.
Rafkin, S.C.R., Michaels, T.I., 2003. Meteorological predictions for 2003 Mars Exploration Rover high-priority landing sites. J. Geophys. Res. 108, 8091. http://dx.doi.org/10.1029/2002JE002027.
Rafkin, S.C.R., Haberle, R.M., Michaels, T.I., 2001. The Mars Regional Atmospheric Modeling System: Model Description and selected simulations. Icarus 151, 228–256.
Reiss, D., Raack, J., Rossi, A.P., Di Achille, G., Hiesinger, H., 2010. First in situ analysis of dust devil tracks on Earth and their comparison with tracks on Mars. Geophys. Res. Lett. 37, L14203. http://dx.doi.org/10.1029/2010GL044016.
Reiss, D., Raack, J., Hiesinger, H., 2011a. Bright dust devil tracks on Earth: Implications for their formation on Mars. Icarus 211, 917–920.
Reiss, D., Zanetti, M., Neukum, G., 2011b. Multitemporal observations of identical active dust devils on Mars with the High Resolution Stereo Camera (HRSC) and Mars Orbiter Camera (MOC). Icarus 215, 358–369.
Rennó, N.O., Burkett, M.L., Larkin, M.P., 1998. A simple thermodynamical theory for dust devils. J. Atmos. Sci. 55, 3244–3252.
Ryan, J.A., Lucich, R.D., 1983. Possible dust devils, vortices on Mars. J. Geophys. Res. 88, 11005–11011.
Seelos and the CRISM Team, 2009. CRISM Data Users' Workshop Nili Fossae Data Processing Walkthrough. Introduction to CAT Presentation from 3/22/09 Workshop, the Woodlands, TX, USA. <http://pds-geosciences.wustl.edu/workshops/CRISM_Workshop_Mar09_presentations/CRISM_Workshop_090322_Nili_Fossae_Walkthrough_FPS.pdf>.
Spiga, A., 2012. Comment on "Observing desert dust devils with a pressure logger" by Lorenz (2012) – Insights on measured pressure fluctuations from large-eddy simulations. Geosci. Instrum. Methods Data Syst. 1, 151–154.
Spiga, A., Forget, F., 2009. A new model to simulate the martian mesoscale and microscale atmospheric circulation: Validation and first results. J. Geophys. Res. 114, E02009. http://dx.doi.org/10.1029/2008JE003242.
Stanzel, C., Pätzold, M., Greeley, R., Hauber, E., Neukum, G., 2006. Dust devils on Mars observed by the High Resolution Stereo Camera. Geophys. Res. Lett. 33, L11202. http://dx.doi.org/10.1029/2006GL025816.
Stanzel, C., Pätzold, M., Williams, D.A., Whelley, P.L., Greeley, R., Neukum, G.the HRSC Co-Investigator Team, 2008. Dust devil speeds, directions of motion and general characteristics observed by the Mars Express High Resolution Stereo Camera. Icarus 197, 39–51.
Thomas, P., Gierasch, P.J., 1985. Dust devils on Mars. Science 230, 175–177.
Toigo, A.D., Richardson, M.I., Ewald, S.P., Gierasch, P.J., 2003. Numerical simulation of martian dust devils. J. Geophys. Res. 108, 5047. http://dx.doi.org/10.1029/2002JE002002.
Torson, J.M., Becker, K.J., 1997. ISIS – A software architecture for processing planetary images. Lunar Planet. Sci. XXVIII, 1443–1444 (abstract).
Tyler, D., Barnes, J.R., Haberle, R.M., 2002. Simulation of surface meteorology at the Pathfinder and VL1 sites using a Mars mesoscale model. J. Geophys. Res. 107, 5018. http://dx.doi.org/10.1029/2001JE001618.
Wegener, A., 1914. Staubwirbel auf Island. Meteorol. Z. 31, 199–200.
Whelley, P.L., Greeley, R., 2008. The distribution of dust devil activity on Mars. J. Geophys. Res. 113, E07002. http://dx.doi.org/10.1029/2007JE002966.